General analytic theory of classical collinear three-wave mixing in a monolithic cavity

OPEN ACCESS
IOP Publishing
Journal of Optics
J. Opt. **23** (2021) 085803 (5pp)
https://doi.org/10.1088/2040-8986/ac0b90

General analytic theory of classical collinear three-wave mixing in a monolithic cavity

Matteo Santandrea*, **Michael Stefszky** and **Christine Silberhorn**

Paderborn University, Integrated Quantum Optics Group, Institute for Photonic Quantum Systems (PhoQS), Warburger Straße 100, Paderborn 33098, Germany

E-mail: matteo.santandrea@upb.de

Received 26 March 2021, revised 26 May 2021
Accepted for publication 15 June 2021
Published 24 August 2021

Abstract

Integrated, monolithic nonlinear cavities are of great interest in both classical and quantum optics experiments due to their high efficiency and stability. However, a general analytic theory of classical three-wave mixing in such monolithic systems, including both linear and nonlinear regions with arbitrary finesse and non-zero propagation losses, is a challenging task. Here, we derive such a model for any three-wave mixing process (second harmonic, sum frequency and difference frequency generation) under the sole assumption of low single-pass conversion efficiency. We demonstrate remarkable agreement between the presented model and the experimentally obtained highly complex second-harmonic spectrum of a titanium-indiffused lithium niobate waveguide cavity that includes both a linear and nonlinear section. We then show the effect that reversing the linear and nonlinear regions has on the output spectrum, highlighting the importance of system design. Finally, we demonstrate that the model can be extended to include the effect of phase modulation applied to the cavity.

Keywords: nonlinear optics, monolithic cavity, three wave mixing, phase modulators

1. Introduction

Integrated devices offer greater stability, easier interfacing to fiber networks and smaller footprint than their bulk counterparts [1]. The functionality of these devices can be extended by incorporating a wide variety of linear (e.g. directional couplers and phase shifters) and nonlinear (e.g. second harmonic generation stage and polarization converter) components on the chip [2, 3]. This flexibility makes integrated nonlinear optical devices a key component of many classical and quantum optical experiments.

In recent years, integrated monolithic cavities have gained increasing interest, in particular in the quantum optics community [4–11]. They enable the generation of pure parametric downconverted states [12], optical frequency combs [13], and squeezed states of light [14], and can be used as interconnecting blocks for interfacing with narrowband quantum memories [15].

Such advantages come with a price, namely an increased complexity of the integrated structure and less access to certain degrees of freedom to address this increased complexity. In particular, many recent nonlinear integrated cavities report the presence of a nonlinear section surrounded by electro-optic [16] or thermo-optic and piezo-optic [15] modulators. This allows for a fine-tuning of the resonance conditions, but results in a more complex interaction between the three fields inside the cavity that cannot be addressed using more standard bulk dispersion compensation techniques, such as using a wedged crystal [17, 18].

To date, the main method to study these systems is based on the model developed by Berger in reference [19]. However,

* Author to whom any correspondence should be addressed.

this model only considers type 0 second harmonic generation (SHG) in a cavity comprising only a single nonlinear region, and therefore it cannot be directly extended to the wider class of nonlinear integrated cavities described above. An improvement over Berger's model is found in [15], where the authors model a type 0 SHG cavity with thermo-optic modulators surrounding the nonlinear region. However, the model derived cannot be easily extended to different system configurations (e.g. type II SHG or sum frequency generation). Moreover, they neglect the impact of losses on the fundamental field, a condition that is reasonable for their bulk system but that cannot be generalized, e.g. to waveguide resonators.

In this paper, we expand the model of [19] and [15] and provide a comprehensive analytical model of three-wave mixing processes in nonlinear cavities under the non-pump depletion approximation. This general model is valid for SHG, sum frequency generation (SFG) and difference frequency generation (DFG) processes, and therefore can also be used to derive useful insights into parametric downconversion (PDC) in cavities. We derive the equation describing the spectrum of light generated in the cavity through a chosen nonlinear process and show that our model accurately reproduces experimental measurements performed on titanium-diffused lithium niobate waveguides.

2. Analytic theory

Let us consider the system of length $L_{\text{tot}} = L_1 + L_2 + L_3$ sketched in figure 1, composed of a nonlinear region of length L_2 surrounded by two regions without nonlinearity of length L_1 and L_3. Two input fields E_1 and E_2, at frequencies ω_1 and ω_2, enter the system from the left facet and generate the field E_3 at frequency ω_3 in the central nonlinear region. Due to the non-zero facet (amplitude) reflection coefficients $\rho_{1,2,3}$ (with corresponding transmission coefficients $\tau_{1,2,3}$), the three fields interfere with themselves as they propagate back and forth through the sample. Therefore, the spectrum of the generated field E_3 will be the result of the phase-matching properties of the nonlinear region as well as the resonance conditions of the three fields, which we now aim to describe. An analytic solution for the spectrum $E_3(\omega_3)$ can be found under the assumption that the input fields $E_{1,2}$ are undepleted by the nonlinear process. Removing this assumption is possible, but the solution requires a numerically based iterative approach [20].

We start by considering the evolution of the fields E_1 and E_2, which enter the system from the left facet. Parameters pertaining to the left facet are denoted by a superscript 'left', while parameters pertaining to the right facet are denoted by a superscript 'right'. Under the non-depletion approximation, the steady-state circulating fields $E_{1,\text{circ}}$ and $E_{2,\text{circ}}$ inside the cavity, calculated at the left facet of the system, can be written as a function of the input fields $E_{1,\text{input}}$ and $E_{2,\text{input}}$ as given by the usual Fabry–Pérot resonance condition

$$E_{j,\text{circ}} = \frac{\tau_j^{\text{left}}}{1 - \rho_j^{\text{left}}\rho_j^{\text{right}} e^{-2\,i\phi_{\text{FP},j}}} E_{j,\text{input}} \qquad j = 1,2 \qquad (1)$$

where $\phi_{\text{FP},j}$ is the complex phase factor acquired by the field j over a single round trip of the cavity, which is given by

$$\begin{aligned} \phi_{\text{FP},j} &= \phi_{j,1} + \phi_{j,2} + \phi_{j,3} \\ \phi_{j,l} &= (\beta_{j,l} - i\alpha_j/2) L_l \qquad l = 1,2,3. \end{aligned} \qquad (2)$$

Here, $\beta_{j,l} = 2\pi n_{j,l}/\lambda_j$ is the propagation constant of field j in region l and α_j is the intensity propagation losses of field j. The refractive index of field j in region l is given by $n_{j,l}$ and its wavelength is given by λ_j. We consider the propagation constants in the three regions to be independent, allowing the description of systems with active elements that can modify the phase relationship between the fields, e.g. electro-optic or thermo-optic modulators.

The next step involves tracking the evolution of the field E_3 along a single round trip of the cavity. A second subscript on the fields E_1, E_2 and E_3 is used to denote their location in the cavity, as illustrated in figure 1. Since we assume steady-state conditions, we can relate the field after a single round trip to the starting field. This leads to the following self-consistent system of equations

$$\begin{cases} E_{3,2} = E_{3,1} e^{-i\phi_{3,1}} \\ E_{3,3} = \text{NL}(L_2; E_{1,2}, E_{2,2}, E_{3,2}) e^{-i\beta_{3,2}L_2} \\ E_{3,4} = E_{3,3} e^{-i\phi_{3,3}} \\ E_{3,5} = \rho_3^{\text{right}} E_{3,4} \\ E_{3,6} = E_{3,5} e^{-i\phi_{3,1}} \\ E_{3,7} = \text{NL}(L_2; E_{1,6}, E_{2,6}, E_{3,6}) e^{-i\beta_{3,2}L_2} \\ E_{3,8} = E_{3,7} e^{-i\phi_{3,1}} \\ E_{3,1} = \rho_3^{\text{left}} E_{3,8} \end{cases} \qquad (3)$$

where

$$\begin{aligned} E_{1,2} &= E_{1,\text{circ}} e^{-i\phi_{1,1}} \\ E_{2,2} &= E_{2,\text{circ}} e^{-i\phi_{2,1}} \\ E_{1,6} &= E_{1,\text{circ}} e^{-i(\phi_{1,1}+\phi_{1,2}+2\phi_{1,3})} \\ E_{2,6} &= E_{2,\text{circ}} e^{-i(\phi_{2,1}+\phi_{2,2}+2\phi_{2,3})} \end{aligned} \qquad (4)$$

are values of the fields E_1 and E_2 at the input of the nonlinear section, in the forward ($E_{1,2}$ and $E_{2,2}$) and in the backward ($E_{1,6}$ and $E_{2,6}$) direction.

In equation (3), the notation $\text{NL}(L; E_1, E_2, E_3)$ has been used to indicate the complex amplitude of the field E_3 generated in a section L of nonlinear material, with initial conditions E_1, E_2 and E_3. In the case of SFG, where $\omega_3 = \omega_1 + \omega_2$, the evolution of the field E_3 can be evaluated by solving the coupled system of equations

$$\begin{aligned} \frac{dE_1}{dz} &= -\frac{\alpha_1}{2} E_1 \\ \frac{dE_2}{dz} &= -\frac{\alpha_2}{2} E_2 \\ \frac{dE_3}{dz} &= i\gamma E_1 E_2 e^{i\Delta\beta z} - \frac{\alpha_3}{2} E_3. \end{aligned} \qquad (5)$$

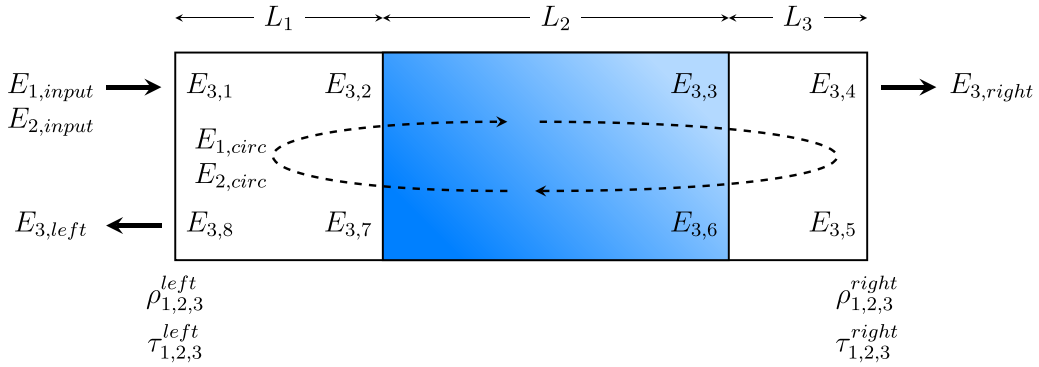

Figure 1. Sketch of the system described by equations (3) and (4).

In equation (5), γ is the nonlinear coupling coefficient between the three fields and includes constants such as the nonlinearity of the system and the modal overlap between the three fields [21], while $\Delta\beta = \beta_{3,2} - \beta_{2,2} - \beta_{1,2} - \beta_G$ is the wavevector mismatch with propagation constants as defined in (2). Here, $\beta_G = \frac{2\pi}{\Lambda}$ is the additional quasi-phase-matching grating vector, which needs to be considered in samples where the nonlinearity is periodically inverted, with period Λ.

The solution of equation (5) over a nonlinear region of length L and with initial conditions $E_{1,0}, E_{2,0}, E_{3,0}$ can be found analytically, resulting in

$$\begin{aligned} E_3(L) &= \mathrm{NL}_3(L; E_{1,0}, E_{2,0}, E_{3,0}) \\ &= \mathrm{i}\gamma E_{1,0}E_{2,0}L\,\mathrm{sinc}\left(\frac{\overline{\Delta\beta}L}{2}\right)\mathrm{e}^{\mathrm{i}\frac{\overline{\Delta\beta}L}{2}}\mathrm{e}^{-\frac{\alpha_3}{2}L} + E_{3,0}\mathrm{e}^{-\frac{\alpha_3}{2}L}, \end{aligned} \tag{6}$$

where $\overline{\Delta\beta}$ is given by

$$\overline{\Delta\beta} = \Delta\beta - \mathrm{i}(\alpha_3 - \alpha_2 - \alpha_1)/2. \tag{7}$$

The self-consistent system (3) and the phase-matching equation (6) allow us to retrieve the value of the field E_3 propagating inside the cavity. Finally, we can propagate the intra-cavity field E_3 to the external fields outside the cavity via the amplitude transmission coefficients τ_3. The resulting electric fields can be described as follows

$$\begin{aligned} E_3^{\mathrm{out,right}} &= \tau_3^{\mathrm{right}}\tau_1^{\mathrm{left}}\tau_2^{\mathrm{left}}E_{1,\mathrm{input}}E_{2,\mathrm{input}}\cdot\mathrm{PM}\cdot\mathrm{FP}_1\cdot\mathrm{FP}_2\cdot\mathrm{FP}_3\cdot\Phi_r \\ E_3^{\mathrm{out,left}} &= \tau_3^{\mathrm{left}}\tau_1^{\mathrm{left}}\tau_2^{\mathrm{left}}E_{1,\mathrm{input}}E_{2,\mathrm{input}}\cdot\mathrm{PM}\cdot\mathrm{FP}_1\cdot\mathrm{FP}_2\cdot\mathrm{FP}_3\cdot\Phi_l \end{aligned} \tag{8}$$

with

$$\begin{aligned} \mathrm{PM} &= \mathrm{i}\gamma L_2\,\mathrm{sinc}\left(\frac{\overline{\Delta\beta}L_2}{2}\right)\mathrm{e}^{\mathrm{i}\frac{\overline{\Delta\beta}L_2}{2}} \\ \mathrm{FP}_j &= \frac{1}{1-\rho_j^{\mathrm{left}}\rho_j^{\mathrm{right}}\mathrm{e}^{-2\,\mathrm{i}\phi_{\mathrm{FP},j}}}, \qquad j = 1,2,3 \\ \Phi_r &= \mathrm{e}^{-\mathrm{i}(\phi_{1,1}+\phi_{2,1}+\phi_{3,2}+\phi_{3,3})} \\ &\quad\times(1+\rho_1^{\mathrm{right}}\rho_2^{\mathrm{right}}\rho_3^{\mathrm{left}}\mathrm{e}^{-\mathrm{i}(2\phi_{3,1}+\phi_{1,2}+\phi_{2,2}+\phi_{3,2}+2\phi_{1,3}+2\,\phi_{2,3})}) \\ \Phi_l &= \mathrm{e}^{-\mathrm{i}(\phi_{1,1}+\phi_{2,1}+\phi_{3,1}+\phi_{1,2}+\phi_{2,2}-2\phi_{\mathrm{FP},1}-2\phi_{\mathrm{FP},2}-2\phi_{\mathrm{FP},3}))} \\ &\quad\times\left(\rho_1^{\mathrm{right}}\rho_2^{\mathrm{right}}\mathrm{e}^{\mathrm{i}(\phi_{3,2}+2\phi_{3,3})}+\rho_3^{\mathrm{right}}\mathrm{e}^{\mathrm{i}(\phi_{1,2}+\phi_{2,2}+2\phi_{1,3}+2\phi_{2,3})}\right) \end{aligned} \tag{9}$$

Equations (8) and (9) represent the main result of our work. In writing equation (8), the different factors determining the spectrum of E_3 outside the cavity have been separated according to their source: the term PM represents the (single-pass) phase-matching spectrum of the nonlinear section L_2, the terms $\mathrm{FP}_{1/2/3}$ represent the contributions of the Fabry–Pérot cavities of the three fields, and the terms $\Phi_{r/l}$ represent the interference between the forward and backward generated E_3 fields. In the next section, we show how this model accurately models the response of a real cavity system.

3. Application to a real system

Here, we model the spectral properties of the double pass second harmonic cavity system presented in [16]. The device consists of a ∼2 cm-long waveguide comprising a ∼1 cm-long unpoled region with an electro-optic phase modulator on the left (input) side followed by a ∼1 cm-long poled region for second harmonic generation pumped at 1540 nm on the right (output) side.

Dielectric coatings are deposited on the waveguide facets, such that the waveguide acts as a high-finesse resonator for the fundamental field and a double-pass structure for the second harmonic field. The input facet is chosen to have a 70% (intensity) reflectivity for the fundamental field and a high reflectivity coating for the second harmonic, while the output facet has a high reflectivity coating for the fundamental field and an anti-reflection coating for the second harmonic field. The measured values for the reflection coefficients ρ and the propagation losses α_{FF} for the fundamental field are summarized in table 1. The losses α_{SH} of the second harmonic field are difficult to characterize as the waveguide is multimode at this frequency and thus they are assumed to be twice as high as the fundamental losses. We also note that, due to the double-pass configuration, the second harmonic losses will only have a minor impact on the output spectrum of the device.

Under these assumptions, it is possible to calculate the phase-matching spectrum of the waveguide cavity using

Table 1. Values of the reflection coefficients and fundamental losses used to model the system presented in [16].

ρ_{FF}^{left}	ρ_{FF}^{right}	ρ_{SH}^{left}	ρ_{SH}^{right}	α_{FF}	α_{SH}
0.833	0.998	0.998	0.1	0.25 dB cm^{-1}	0.5 dB cm^{-1}

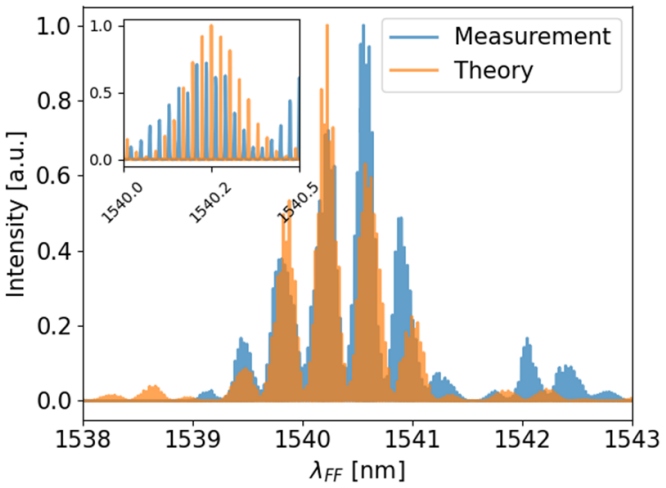

Figure 2. Measured phase-matching spectrum of the double-pass SHG device reported in reference [16] and its theoretical model found using equation (8). The inset shows the longitudinal modes of the generated SH field, the spacing of which is given by the free spectral range of the SH cavity.

equations (8) and (9). A comparison between the measured phase-matching spectrum and the theoretical model is shown in figure 2. Our model can capture remarkably well most of the characteristics of the measured spectrum, namely, the position, the width and the complex envelope structure of the interference pattern. The discrepancies between the theoretical and the measured spectra arise from the difficulty in estimating the exact length of each section and from the inhomogeneities present in the sample. More specifically, errors in estimating the length of the different sections will affect both the free spectral range of the system and the interference between the three waves, while it is known that waveguide inhomogeneities may lead to an asymmetric phase-matching profile [16, 22, 23].

The theory developed in the previous section allows us to investigate the impact that system design has on device performance. As an example, we investigate the impact that swapping the order of the phase modulator and the nonlinear region has on the output spectrum. The resulting phase-matching spectra are shown in figure 3. We can see that the spectrum of the sample with the phase modulator before the nonlinear region (as is the case for the system presented in [16]) is characterized by a periodic modulation of the envelope, which is absent in the opposite configuration. This is due to the fact that in this case the phase modulator is placed between the SH field that is generated in the reverse and the forward direction, noting that nearly all the SH field exits the sample at the right mirror. Therefore, driving the phase modulator also varies the interference conditions between these two waves,

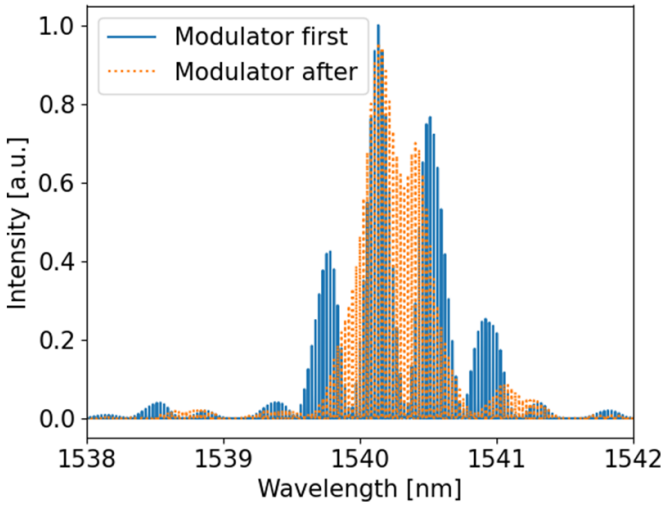

Figure 3. Expected phase-matching spectra for the sample presented in [16] and modeled with the parameters reported in table 1, depending on the position of the phase modulator with respect to the nonlinear region.

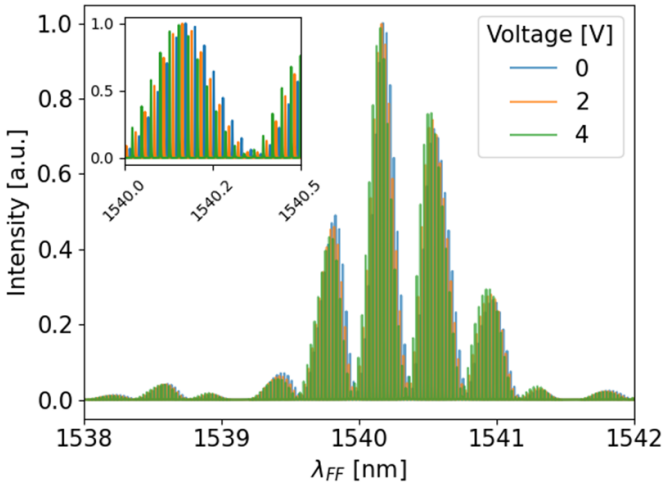

Figure 4. Predicted shift of the phase-matching spectrum with various voltages applied to the electro-optic modulator for the sample presented in [16] and modeled with the parameters reported in table 1.

leading to regions of destructive interference. This reveals that the resonance conditions in the first configuration are much stricter and, depending on the application, may impact device performance. This highlights the importance of careful design and modeling of these systems.

Finally, this model also allows us to calculate the effect that driving the phase modulator has on the output phase-matching spectrum. This is achieved by writing the refractive index of the fields in the first region, i.e. where the electro-optic modulator is located, as

$$n(V) = n_e - \frac{n_e^3}{2} r \frac{V}{d} \Gamma \tag{10}$$

where r is the electro-optic coefficient addressed by the phase modulator (in this case, it corresponds to $r_{33} = 30.8$pm/V), V

is the voltage applied to the electrodes of the modulator, d is the distance between the electrodes, n is the extraordinary refractive index of the waveguide in the absence of any electric field, and Γ is the overlap integral between the field of the modulator and the one of the guided mode.

When a non-zero voltage is applied to the modulator, the phase of both the fundamental and second harmonic fields varies, thus changing the interference conditions inside the cavity. This results in a shift in the position of the resonance peaks of the structure as well as a variation of the maximum intensity of the generated light due to the complex interaction of the three fields inside the resonator as their phase relationship is altered by the driven modulator. This is illustrated in figure 4 for three different applied voltage levels.

4. Conclusions

In this paper, we have presented a general analytic theory of an integrated cavity comprising linear and nonlinear sections under the sole approximation of no pump depletion. The presented model is general and can be applied to any type of collinear three-wave mixing process— both in bulk and in waveguides. We have demonstrated that it accurately reproduces experimental data and shown its capabilities in modeling the effect of integrated modulators on the phase-matching spectrum of the device. This model constitutes a fundamental step toward the understanding and optimization of the performance of a wide variety of new, complex resonant nonlinear devices for both classical and quantum optics applications.

Funding

Deutsche Forschungsgemeinschaft (SI 1115/6-1).

Data availability statement

The data that support the findings of this study are available upon reasonable request from the authors.

ORCID iDs

Matteo Santandrea https://orcid.org/0000-0001-5718-358X
Michael Stefszky https://orcid.org/0000-0001-5379-3460
Christine Silberhorn https://orcid.org/0000-0002-2349-5443

References

[1] Orieux A and Diamanti E 2016 Recent advances on integrated quantum communications *J. Opt.* **18** 083002
[2] Lenzini F *et al* 2018 Integrated photonic platform for quantum information with continuous variables *Sci. Adv.* **4** 1–8
[3] Luo K H, *et al* 2018 Nonlinear integrated quantum electro-optic circuits *Sci. Adv.* **5** 1–8
[4] Yonezawa H, Nagashima K and Furusawa A 2010 Generation of squeezed light with a monolithic optical parametric oscillator: simultaneous achievement of phase matching and cavity resonance by temperature control *Opt. Express* **18** 20143–50
[5] Phillips C R, Pelc J S and Fejer M M 2011 Continuous wave monolithic quasi-phase-matched optical parametric oscillator in periodically poled lithium niobate *Opt. Lett.* **36** 2973–5
[6] Horn R, *et al* 2012 Monolithic source of photon pairs *Phys. Rev. Lett.* **108** 153605
[7] Raymer M G and McKinstrie C J 2013 Quantum input-output theory for optical cavities with arbitrary coupling strength: application to two-photon wave-packet shaping *Phys. Rev.* A **88** 043819
[8] Brieussel A *et al* 2016 Squeezed light from a diamond-turned monolithic cavity *Opt. Express* **24** 4042–56
[9] Zhang M, *et al* 2017 Monolithic ultra-high-q lithium niobate microring resonator *Optica* **4** 1536–7
[10] Alsing P M and Hach E E 2017 Photon-pair generation in a lossy microring resonator. i. theory *Phys. Rev.* A **96** 033847
[11] Yao N *et al* 2018 Lithium niobate micro-disk resonators of quality factors above 10^7 *Opt. Lett.* **43** 4116
[12] Luo K H *et al* 2015 Direct generation of genuine single-longitudinal-mode narrowband photon pairs *New J. Phys.* **17** 073039
[13] Stefszky M*et al* 2018 Towards optical-frequency-comb generation in continuous-wave-pumped titanium-indiffused lithium-niobate waveguide resonators *Phys. Rev.* A **98** 1–9
[14] Stefszky M *et al* 2017 Waveguide cavity resonator as a source of optical squeezing *Phys. Rev. Appl.* **7** 1–5
[15] Zielińska J A *et al* 2017 Fully-resonant, tunable, monolithic frequency conversion as a coherent UVA source *Opt. Express* **25** 1142–50
[16] Stefszky M *et al* 2021 Waveguide resonator with an integrated phase modulator for second harmonic generation *Opt. Express* **29** 1991–2002
[17] Imeshev G, Proctor M and Fejer M M 1998 Phase correction in double-pass quasi-phase-matched second-harmonic generation with a wedged crystal *Opt. Lett.* **23** 165
[18] Stefszky M *et al* 2010 An investigation of doubly-resonant optical parametric oscillators and nonlinear crystals for squeezing *J. Phys. B: At. Mol. Opt. Phys.* **44** 015502
[19] Berger V 1997 Second-harmonic generation in monolithic cavities *J. Opt. Soc. Am.* B **14** 1351–60
[20] Fujimura M, Suhara T and Nishihara H 1996 Theoretical analysis of resonant waveguide optical second harmonic generation *J. Lightwave Technol.* **14** 1899–906
[21] Jankowski M, Mishra J and Fejer M M 2021 Dispersion-engineered $\chi^{(2)}$ nanophotonics: a flexible tool for nonclassical light (arXiv:2103.02296)
[22] Helmfrid S and Arvidsson G 1991 Influence of randomly varying domain lengths and nonuniform effective index on second-harmonic generation in quasi-phase-matching waveguides *J. Opt. Soc. Am.* B **8** 797–804
[23] Santandrea M *et al* 2019 Fabrication limits of waveguides in nonlinear crystals and their impact on quantum optics applications *New J. Phys.* **21** 033038